Spin Crossover

International Edition: DOI: 10.1002/anie.201411309
German Edition: DOI: 10.1002/ange.201411309

The Kinetic Isotope Effect as a Probe of Spin Crossover in the C–H Activation of Methane by the FeO^+ Cation**

*Binh Khanh Mai and Yongho Kim**

Abstract: *Two-state reactivity (TSR) is often used to explain the reaction of transition-metal–oxo reagents in the bare form or in the complex form. The evidence of the TSR model typically comes from quantum-mechanical calculations for energy profiles with a spin crossover in the rate-limiting step. To prove the TSR concept, kinetic profiles for C–H activation by the FeO^+ cation were explored. A direct dynamics approach was used to generate potential energy surfaces of the sextet and quartet H-transfers and rate constants and kinetic isotope effects (KIEs) were calculated using variational transition-state theory including multidimensional tunneling. The minimum energy crossing point with very large spin–orbit coupling matrix element was very close to the intrinsic reaction paths of both sextet and quartet H-transfers. Excellent agreement with experiments were obtained when the sextet reactant and quartet transition state were used with a spin crossover, which strongly support the TSR model.*

Methanol is one of the top 25 chemicals produced worldwide and has been proposed as a liquid fuel.[1] Much attention has been paid in applied and pure chemistry to the direct method to convert methane to methanol with efficient catalysts.[2] In 1990, Schröder and Schwarz[3] reported that under thermal conditions, methane-to-methanol conversion can occur when the gas-phase FeO^+ cation is used as a catalyst. Fiedler et al.[4] suggested that this methane-to-methanol conversion is involved in more than one state, and the spin inversion occurs at the crossing region of two potential energy surfaces of different spin states, which can help to decrease the barrier height and increase the efficiency of this conversion. This phenomenon can be called a "two-state reactivity" (TSR) and has been proposed by Shaik and coworkers.[5] This idea has been applied to later theoretical studies by Yoshizawa[6] and Metz[7] with the same reaction. Other examples for spin-forbidden reactions in an organometallic reaction were also reported by Harvey et al.[8] The TSR model has been widely used to explain the reactivity of many organometallic and bioinorganic systems.[9] However, the evidence for the TSR model came primarily from quantum mechanical studies showing the crossing of simple one-dimensional potential energy profiles in the rate-determining step. Because it is very difficult to accurately predict the energetics of transition-metal complexes of two different spin states,[10] there is still some debate whether the spin crossover plays an important role.

The kinetic isotope effect (KIE) is in principle determined by the transition state (TS) properties and the shape of the potential energy surface, which depends on the spin state of the reactions; therefore, theoretical investigation of KIEs in comparison with experiments can be used to test whether the spin crossover played an important role in the methane hydroxylation by FeO^+. Herein, we present variational transition-state theory calculations including multidimensional tunneling (VTST/MT) to reproduce the kinetic signatures of this reaction, such as rate constants and KIEs for the hydrogen atom transfer (HAT) based on quantum mechanically generated intrinsic reaction coordinates (IRCs). This approach has recently been applied successfully to study C–H activation reactions by transition-metal complexes.[11] The direct dynamics approach, where energies and frequencies are calculated as needed on the potential energy surface, was used to generate the potential energy surface at the B3LYP/def2-TZVPP level, and the IRC was obtained by following the minimum energy path (MEP) from the TS to either the reactant or product using the Page–McIver method.[12] Altun et al.[13] recently demonstrated that the B3LYP functional shows very good benchmark results for the energetics of similar reactions.

The potential energy profile and some bond lengths and angles of stationary point structures are shown in Figure 1 and 2, respectively. Methane hydroxylation occurs via two-step mechanisms through the formation of a hydroxyl intermediate $[H_3C\text{-}Fe\text{-}OH]^+$. The relative energetics in this study are quite similar to those of previous high-level quantum mechanical studies, and clearly indicates crossing of two spin state energies between the reactant complex (RC) and TS.

The $FeO{-}CH_4$ complexes had an η^3 configuration with three C–H bonds pointing toward Fe, and the binding energies were 30.7 and 23.4 kcal mol^{-1} for the quartet and sextet spin state, respectively. The donor–acceptor interaction energies between C–H σ-orbitals and Fe–O antibonding orbitals (both σ*- and π*-orbitals) were calculated using the natural bond orbital analysis,[14] and 20.8 and 15.8 kcal mol^{-1} were obtained for the quartet and sextet, respectively. The back-bonding energies between FeO and CH_4 were calculated from the interaction energies between Fe–O bonding orbitals and C–H σ*-orbitals, which were approximately 2 kcal mol^{-1} for both spin states. These results suggest that the donor–acceptor interaction between C–H bonding and Fe–O antibonding orbitals, which is the stabilization energy owing to

[*] B. K. Mai, Prof. Dr. Y. Kim
Department of Applied Chemistry and Institute of Applied Sciences
Kyung Hee University, Yongin-Si, Gyeonggi-Do, 446-701 (Korea)
E-mail: yhkim@khu.ac.kr

[**] This work was supported by a grant from Korea Research Foundation (NRF Grant No. 2010-0012990).

Supporting information for this article is available on the WWW under http://dx.doi.org/10.1002/anie.201411309.

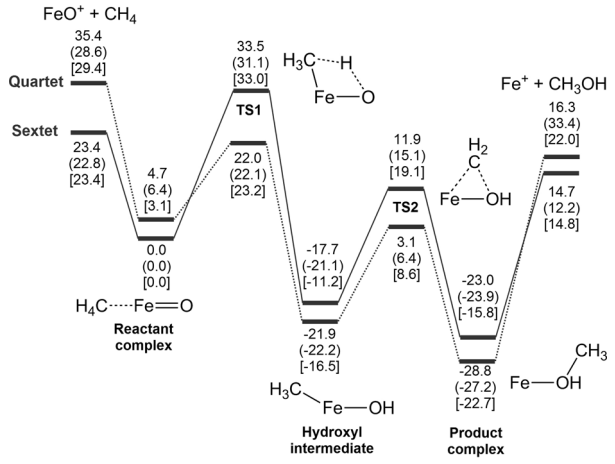

Figure 1. Potential-energy diagram for the C–H activation by FeO^+ cation at the B3LYP/def2-TZVPP level. The numbers in the parenthesis and square brackets are at the B3LYP/6-311G**[6c] and CBS-QB3[7] levels, respectively. All values are in kcal mol^{-1}.

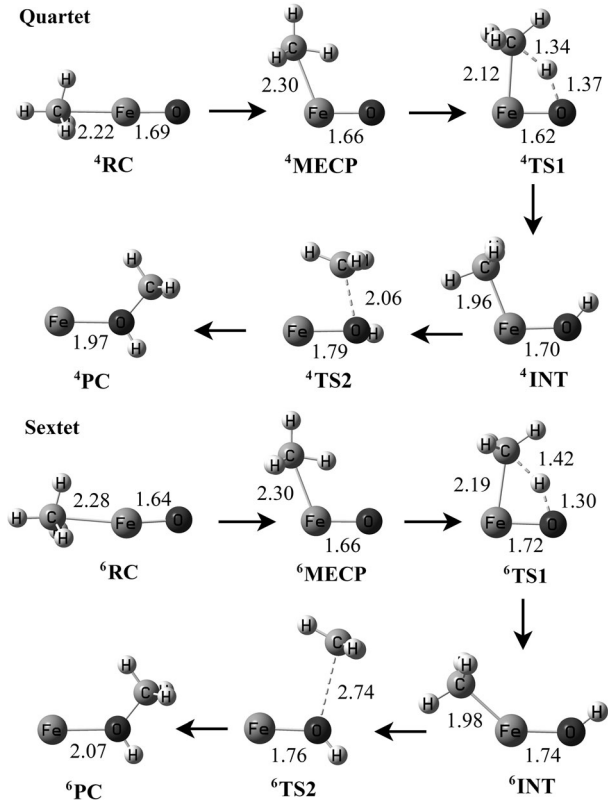

Figure 2. Stationary point structures for the CH_4 activation by FeO^+ cation at quartet and sextet spin states calculated at the B3LYP/def2-TZVPP level. All number are in Å.

partial charge-transfer from bonding to antibonding orbitals, is the main factor for the binding of CH_4 to FeO^+. The C-Fe-O angles were 177° and 166° at the quartet and sextet, respectively. During the HAT, the C-Fe-O angle decreased gradually and became smaller than 90° at TS1. TS1 had a four-membered ring structure, where the C–H and O–H bonds were 1.34 and 1.37 Å, respectively, at the quartet, and 1.42 and 1.30 Å, respectively, at the sextet. When the reaction proceeded from RC to TS1, the Fe–C distance decreased by approximately 0.1 Å for both spin states. However, the Fe–O distances decreased from 1.69 Å to 1.62 Å at the quartet but increased from 1.64 Å to 1.72 Å at the sextet. This opposite trend was probably the most significant spin-dependent structural change along the reaction coordinate. ^{6}RC was lower in energy than ^{4}RC, whereas ^{4}TS1 was lower in energy than ^{6}TS1. Because of the inversion of relative energies for RC and TS1 between two spin states, a spin crossover may occur during the HAT, which is called the two-state reactivity model.

Figure 3 depicts two possible mechanistic scenarios for the spin-state change in the C–H activation by FeO^+; pre-equilibrium between two states ^{6}RC and ^{4}RC and a spin

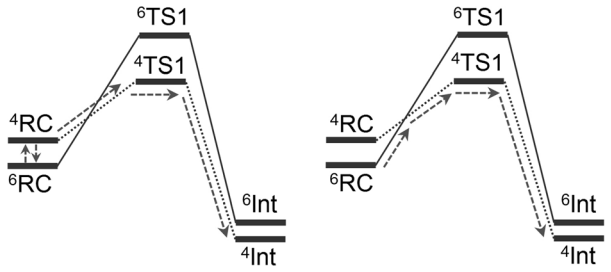

Figure 3. Two possible mechanistic scenarios for a pre-equilibrium and a spin crossover.

crossover during the HAT.[15] The pre-equilibrium mechanism will be supported if the minimum energy crossing point (MECP), where the energy and structure of the two spin states are identical, is far from (or unrelated with) the intrinsic reaction coordinates (IRCs) of HAT, whereas the spin-crossover mechanism is supported if the sextet and quartet IRCs cross at or near the MECP. The MECP was calculated using the Crossing2009 program,[16] where the C-Fe-O angle and Fe–O distance were 111° and 1.66 Å, respectively. The MECP was 8.7 kcal mol^{-1} higher in energy than ^{6}RC.

The sextet and quartet potential and free energy surfaces along the IRCs were calculated (Supporting Information, Figure S1 and S2). Figure 4 depicts the potential energy curves and some geometrical parameters of the FeO^+ complex along the HAT coordinate defined by $q_1 = (r_{CH} - r_{OH})/2$, which represents the dislocation of H between the two end atoms.[17] The energy and geometrical parameters of MECP were included in these plots to show its relation with the IRCs. The V_{MEP} vs. q_1 plots for sextet and quartet crossed at a point with about 8.7 kcal mol^{-1} of energy, which was nearly identical to the relative energy of MECP compared with ^{6}RC. The q_2 vs. q_1 plots for the IRCs of the sextet and quartet were nearly superimposed, where q_2 represents the distance between two end atoms for collinear reaction. However, the r(C–O) vs. q_1 plots for the sextet and quartet were somewhat different and the MECP was in the middle of these two plots. These results showed that the MECP was not exactly on the intrinsic HAT coordinates of either spin states but very close to them, and its energy was also very close to the closest IRCs of the sextet and quartet.

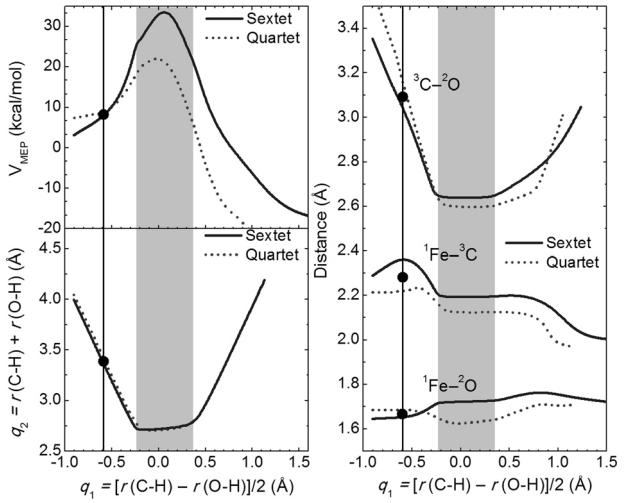

Figure 4. The potential energy curves (top) and some geometrical parameters along the reaction coordinate defined as $q_1 = (r_{CH} - r_{OH})/2$. The vertical lines and filled circles represent the position and individual values of MECP, respectively.

Since the MECP was very close to the IRC of HAT (both geometrically and energetically) and no other low-energy MECP was found, the spin-crossover mechanism is therefore more plausible for this reaction.

The q_2 vs. q_1 plot was nearly flat at approximately $-0.25 < q_1 < 0.35$ Å with $\Delta q_2 \approx 0$, which indicates that the H-atom moved very rapidly between two end atoms, while the end atoms rarely moved. The ^{3}C–^{2}O distance vs. q_1 plot was also nearly flat. The C–H and O–H bonds were being broken and formed, respectively, in this region, without heavy-atom motion. At $q_1 < -0.25$ and $q_1 > 0.35$ Å, two end atoms approach and recede from each other, respectively, without hydrogenic motion. These results indicate that the H atom motion was well separated from the heavy atom motion during the HAT. Tunneling was generally very efficient within this flat region but negligible outside. The MECP appeared far ahead of this flat region, therefore the tunneling coefficient was hardly affected by the spin crossover.

The KIE is very sensitive to the transition-state properties, and the shape of the barrier that depends on the spin state; therefore, KIE can be used as a probe of the spin crossover. Shaik et al.[18] performed quantum mechanical studies for the mechanisms of C–H hydroxylation of *N*,*N*-dimethylaniline in P450 enzymes, and showed that KIE can be used as a probe of the reactive spin state by the comparison of the predicted spin-dependent KIE values with experiments. Harvey[8a,c] has studied kinetics of spin-forbidden reactions and proposed a simple equation for the thermal rate constant of a reaction with the spin crossover through an MECP:

$$k(T) = \langle p_{SI} \rangle \frac{k_B T}{h} \exp\left(-\frac{\Delta G^{\ddagger}}{RT}\right) \quad (1)$$

where $\langle p_{SI} \rangle$ is the mean spin-crossover probability roughly independent of the temperature. For $Fe(CO)_4 + CO$ with 66 cm^{-1} of spin–orbit coupling matrix element,[19] the $\langle p_{SI} \rangle$ value was approximately 0.05. Typical values of $\langle p_{SI} \rangle$ might be in the range of 0.001–0.1 depending on the coupling matrix element, which would increase the activation energy by 1–4 kcal mol^{-1}.[8b] The spin–orbit coupling matrix element at the MECP of this study was 183 cm^{-1} at the CASSCF/def2-TZVPP level, which would introduce quite a large spin-crossover probability. The TS energies of both sextet and quartet states were much greater than the MECP, therefore two spin states of MECP, ^{4}MECP and ^{6}MECP, were thermally equilibrated with each other, and also with the reactant under the approximation of TST. The tunneling coefficient calculations in this study require quantal transmission probabilities at an energy below the top of the barrier; however, this was negligible at the MECP of both spin states (Supporting Information, Figure S3) because of the reason described above.

We divided C–H activation into two parts for rate calculations; the formation of RC and the actual HAT. The equilibrium constants of RC formation and the HAT rate constants are listed in the Supporting Information, Table S1, and the overall rate constants of C–H activation and KIEs are listed in Table 1. The tunneling coefficient, which is very sensitive to the shape of potential energy surfaces, was about 65 times greater for the sextet than the quartet, which will produce quite a different kinetic signature depending on the spin state. Assuming the reaction was to occur in a single spin state without the spin crossover, the rate constants would be very different from the experimental values. The calculated rate constant and KIE of the sextet (^{6}RC–^{6}TS) were much smaller and larger, respectively, than the experimental values. The rate constant of the quartet (^{4}RC–^{4}TS) is also much larger than the experimental value, although the KIE value had the correct order of magnitude. The rate constant and KIE were in the best agreement with experimental values only when the sextet reactants and quartet potential energy surface were used including the transition state (^{6}RC–^{4}TS). This result means that RC and TS1 must have different spin states, the sextet and quartet, respectively, which requires the spin crossover that reduces the barrier height and catalyzes the C–H activation.[9c] Recently, Ard et al.[20] reproduced experimental rate constants and product branching ratios using a statistical model with TS energies as adjustable parameters under the assumption of the spin crossover. We calculated rate constants using VTST/MT based on the B3LYP/def2-TZVPP level potential energy surfaces without any artificial parameters and demonstrated that KIEs were always much larger for ^{6}TS than ^{4}TS irrespective of the spin state of RC

Table 1: Tunneling coefficients (κ), rate constants (cm^3 $molecule^{-1}$ s^{-1}), and KIEs at room temperature.[a]

Spin states	κ [H]	k_{th} [H]	k_{exp} [H]	KIE_{th}[b]	KIE_{exp}[b]
^{6}RC–^{4}TS1	5.35	2.47×10^{-10}	2.0×10^{-10}	4.87	4.6
^{4}RC–^{4}TS1	5.34	3.73×10^{-1}		5.46	
^{6}RC–^{6}TS1	348	8.90×10^{-17}		49.5	
^{4}RC–^{6}TS1	344	1.71×10^{-7}		48.2	

[a] Experimental values are from ref. [3]. [b] Rate constants for H and D transfers are from the CH_2D_2 reactions, which are listed in Table S2.

(Table 1), which suggests that KIE can be used as a sensitive and authentic probe for the spin state of TS and therefore as the evidence of spin crossover. It is tunneling that causes the KIE to be highly spin-dependent; the KIE values rarely changed without tunneling (Supporting Information, Table S2).

To understand why the spin crossover occurs along the HAT, the Hirshfeld spin densities,[21] CM5 partial charge,[22] and atomic valence (number of electrons that an atom uses in bonding) of Fe were monitored along the IRCs of the sextet and quartet, and the results are depicted in Figure 5. The CM5

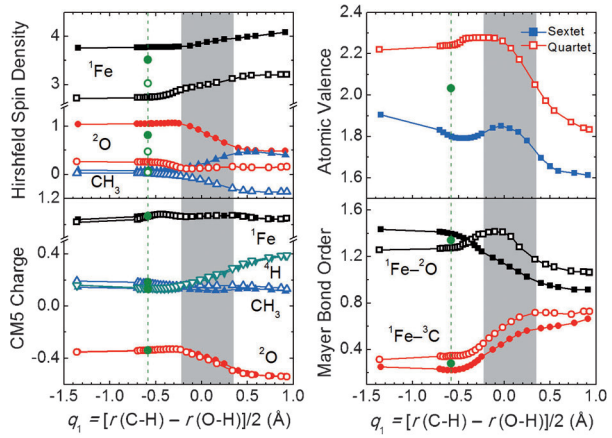

Figure 5. Hirshfeld spin densities, CM5 partial charges, atomic valences of Fe, and Mayer bond orders along the HAT coordinate. The C–H bond breaking and O–H bond formation occurred rapidly in the shaded region with very little heavy atom motion. The closed and open symbols represent sextet and quartet spin states, respectively. The green dashed lines and points represent the positions and individual values of the MECP, respectively.

partial charges of ^{2}O and ^{4}H decreased and increased, respectively, in the shaded region, which suggested that oxygen abstracts an electron from the C–H σ-orbital. However, the partial charges of the two spin states were nearly superimposed, which therefore suggests that the spin-dependent reactivity may not be attributed to the charge density. Furthermore, the spin densities of ^{2}O and CH$_3$ changed differently as the reaction proceeded; the spin density of CH$_3$, for example, increased and decreased for the sextet and quartet, respectively. This indicates that HAT utilizes electrons with different spin depending on the spin state. The spin densities of Fe and ^{2}O, which dropped by nearly one unit at the MECP, and the large increase in the atomic valence of Fe upon the spin crossover, indicate that the spin inversion increases the number of bonding electrons. Interestingly, the two spin densities (sextet and quartet) of MECP were closer than those of IRC at the same q_1 value for both Fe and ^{2}O, and the Fe atomic valence of MECP was in the middle of the sextet and quartet values at the IRC. The ^{2}O spin densities decreased rapidly and were nearly unchanged for the sextet and quartet, respectively, and the Fe atomic valence decreased more rapidly for the sextet than the quartet in the region where the H atom moves very rapidly. The sextet bond orders of ^{1}Fe–^{2}O and ^{1}Fe–^{3}C decreased and increased, respectively, along the IRC. The ^{1}Fe–^{3}C bond order was greater for the quartet than the sextet all along the IRC; however, the quartet bond order of ^{1}Fe–^{2}O started increasing near the MECP, reached a maximum near the TS, and decreased after passing the TS of HAT. These results indicate that the atomic valence of Fe and the associated bond orders, ^{1}Fe–^{2}O and ^{1}Fe–^{3}C, depend significantly on the spin states, which must be closely related to the spin-dependent reactivity.

Shiota and Yoshizawa[6a] suggested that the two-orbital–two-electron interaction between the HOMO orbital of CH$_4$ and the 3σ orbital of FeO$^+$ is the main factor, and this interaction destabilizes the 3σ orbital of the sextet based on the extended Hückel method. The donor–acceptor interaction between the σ_{C-H} and σ^*_{Fe-O} natural bond orbitals, which represent the stabilization energy owing to a partial charge transfer from σ_{C-H} to σ^*_{Fe-O} orbitals, was calculated at several points along the reaction, and the results are depicted in Figure 6. The donor–acceptor interaction energy was approx-

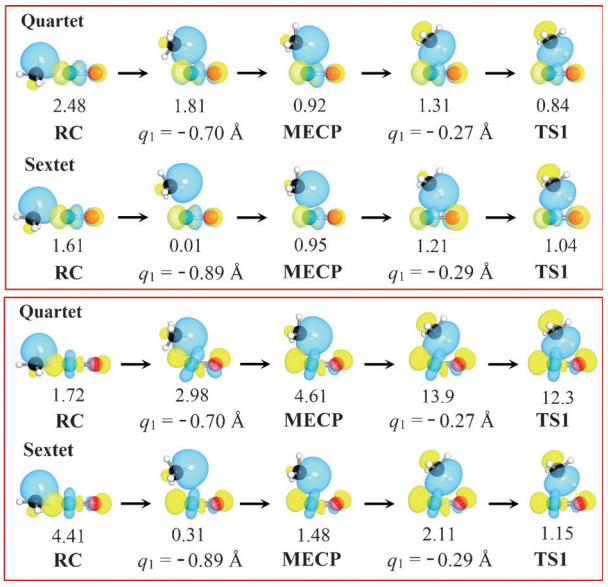

Figure 6. The donor–acceptor interactions for the σ_{C-H} and π^*_{Fe-O} orbitals (top) and the σ_{C-H} and σ^*_{Fe-O} orbitals (bottom) at some points along the HAT coordinate. The numbers are interaction energies in kcal mol^{-1}.

imately 2.7 kcal mol^{-1} greater for ^{6}RC than ^{4}RC. For the sextet, this interaction energy became smaller immediately after the reaction started and rarely changed along the IRC. However, for the quartet, the energy increased rapidly after passing the MECP and became 12 kcal mol^{-1} at TS1. This interaction between σ_{C-H} and π^*_{Fe-O} orbitals were rarely changed during the HAT for both sextet and quartet as depicted in Figure 6. These results mean that the donor–acceptor interaction between σ_{C-H} and σ^*_{Fe-O} orbitals would be the main source of spin-dependent potential energy curves. The spin inversion at the MECP helped to enhance this charge-transfer interaction for the quartet and reduced the barrier height of HAT.

In summary, we calculated the spin-dependent rate constants and KIEs for C–H activation of methane by FeO^+ cation using VTST/MT and demonstrated that the excellent agreement between experimental and predicted KIEs was obtained only when the reactant and transition state had sextet and quartet spin states, respectively, which requires a spin crossover in the reaction. The rate constants were very different from experiments without a spin crossover. The MECP occurred very early in the reaction before the hydrogen was moving and was very close to the IRC. The spin–orbit coupling matrix element of MECP was 183 cm^{-1}, producing a large spin-inversion probability. The donor–acceptor interactions between σ_{C-H} and σ^*_{Fe-O} orbitals were most crucial for the spin-dependent energetics of this reaction. This study demonstrated that experimental rate constants and KIEs along with the theoretical prediction from the VTST/MT could be used as a powerful method to investigate the TSR model, which has been applied for many reactions with transition-metal complexes.

Methods

The structure of all stationary points (reactant, product, intermediate, and TS) were fully optimized at the B3LYP level using the Gaussian 09 program.[23] The def2-TZVPP[24] basis set was used for all atoms. Each minimum and TS structure was confirmed to have zero and one imaginary frequencies, respectively. The MECP between two spin states was located with the Crossing2009 program developed by Harvey.[16] The spin–orbit coupling matrix element between the quartet and sextet spin states was calculated with the Gamess program[25] using the SOC-CI method[26] at the converged CASSCF wavefunction with the same basis set. The CASSCF calculation was performed with the active space of 17 electrons and 12 orbitals. The donor–acceptor interaction was calculated by the NBO analysis using the second-order perturbation theory.[14] All rate calculations were performed with Gaussrate,[27] which is the interface of Gaussian 09 and Polyrate[28] dynamics programs. A direct dynamics approach using the canonical variational transition-state theory (CVT)[29] with microcanonical optimized multidimensional tunneling (μOMT)[30] approximation was used to calculate rate constants and KIEs. Detailed information on the VTST/MT method has been published in several reviews.[31]

Keywords: hydrogen atom transfer · kinetic isotope effect · spin crossover · two-state reactivity · variational transition-state theory

How to cite: *Angew. Chem. Int. Ed.* **2015**, *54*, 3946–3951
Angew. Chem. **2015**, *127*, 4018–4023

[1] G. A. Olah, A. Goeppert, G. K. S. Prakash, *Beyond Oil and Gas: The Methanol Economy*, Wiley, Weinheim, **2009**.
[2] a) H. D. Gesser, N. R. Hunter, C. B. Prakash, *Chem. Rev.* **1985**, *85*, 235–244; b) R. H. Crabtree, *Chem. Rev.* **1995**, *95*, 987–1007; c) D. A. Hickman, L. D. Schmidt, *Science* **1993**, *259*, 343–346; d) R. A. Periana, D. J. Taube, E. R. Evitt, D. G. Löffler, P. R. Wentrcek, G. Voss, T. Masuda, *Science* **1993**, *259*, 340–343; e) L. Shi, G. Yang, K. Tao, Y. Yoneyama, Y. Tan, N. Tsubaki, *Acc. Chem. Res.* **2013**, *46*, 1838–1847.
[3] D. Schröder, H. Schwarz, *Angew. Chem. Int. Ed. Engl.* **1990**, *29*, 1433–1434; *Angew. Chem.* **1990**, *102*, 1468–1469.
[4] A. Fiedler, D. Schroeder, S. Shaik, H. Schwarz, *J. Am. Chem. Soc.* **1994**, *116*, 10734–10741.
[5] a) M. Filatov, S. Shaik, *J. Phys. Chem. A* **1998**, *102*, 3835–3846; b) D. Danovich, S. Shaik, *J. Am. Chem. Soc.* **1997**, *119*, 1773–1786; c) S. Shaik, D. Danovich, A. Fiedler, D. Schröder, H. Schwarz, *Helv. Chim. Acta* **1995**, *78*, 1393–1407.
[6] a) Y. Shiota, K. Yoshizawa, *J. Am. Chem. Soc.* **2000**, *122*, 12317–12326; b) K. Yoshizawa, Y. Shiota, T. Yamabe, *J. Am. Chem. Soc.* **1998**, *120*, 564–572; c) Y. Shiota, K. Yoshizawa, *J. Chem. Phys.* **2003**, *118*, 5872–5879.
[7] G. Altinay, M. Citir, R. B. Metz, *J. Phys. Chem. A* **2010**, *114*, 5104–5112.
[8] a) J.-L. Carreón-Macedo, J. N. Harvey, *J. Am. Chem. Soc.* **2004**, *126*, 5789–5797; b) J. N. Harvey, *WIREs Comput. Mol. Sci.* **2014**, *4*, 1–14; c) J. N. Harvey, *Phys. Chem. Chem. Phys.* **2007**, *9*, 331–343.
[9] a) D. Schröder, S. Shaik, H. Schwarz, *Acc. Chem. Res.* **2000**, *33*, 139–145; b) S. Shaik, H. Hirao, D. Kumar, *Acc. Chem. Res.* **2007**, *40*, 532–542; c) S. Shaik, *Int. J. Mass Spectrom.* **2013**, *354–355*, 5–14.
[10] a) A. Vargas, I. Krivokapic, A. Hauser, L. M. Lawson Daku, *Phys. Chem. Chem. Phys.* **2013**, *15*, 3752–3763; b) L. M. Lawson Daku, F. Aquilante, T. W. Robinson, A. Hauser, *J. Chem. Theory Comput.* **2012**, *8*, 4216–4231; c) S. Ye, F. Neese, *Inorg. Chem.* **2010**, *49*, 772–774; d) A. Ghosh, *J. Biol. Inorg. Chem.* **2006**, *11*, 712–724.
[11] a) K. Park, Y. Pak, Y. Kim, *J. Am. Chem. Soc.* **2012**, *134*, 3524–3531; b) B. K. Mai, Y. Kim, *Chem. Eur. J.* **2013**, *19*, 3568–3572; c) B. K. Mai, Y. Kim, *Chem. Eur. J.* **2014**, *20*, 6532–6541.
[12] M. Page, J. W. McIver, Jr., *J. Chem. Phys.* **1988**, *88*, 922–935.
[13] A. Altun, J. Breidung, F. Neese, W. Thiel, *J. Chem. Theory Comput.* **2014**, *10*, 3807–3820.
[14] a) E. D. Glendening, C. R. Landis, F. Weinhold, *J. Comput. Chem.* **2013**, *34*, 1429–1437; b) F. Weinhold, C. R. Landis, *Valency and Bonding: A Natural Bond Orbital Donor-Acceptor Perspective*, Cambridge University Press, Cambridge, **2005**.
[15] a) H. Hirao, D. Kumar, L. Que Jr., S. Shaik, *J. Am. Chem. Soc.* **2006**, *128*, 8590–8606; b) H. Hirao, L. Que Jr., W. Nam, S. Shaik, *Chem. Eur. J.* **2008**, *14*, 1740; c) N. Harris, S. Shaik, D. Schröder, H. Schwarz, *Helv. Chim. Acta* **1999**, *82*, 1784.
[16] J. N. Harvey, M. Aschi, *Phys. Chem. Chem. Phys.* **1999**, *1*, 5555–5563.
[17] a) H.-H. Limbach, M. Pietrzak, H. Benedict, P. M. Tolstoy, N. S. Golubev, G. S. Denisov, *J. Mol. Struct.* **2004**, *706*, 115–119; b) H.-H. Limbach, J. Miguel Lopez, A. Kohen, *Philos. Trans. R. Soc. London Ser. B* **2006**, *361*, 1399–1415.
[18] a) C. Li, W. Wu, D. Kumar, S. Shaik, *J. Am. Chem. Soc.* **2006**, *128*, 394–395; b) Y. Wang, D. Kumar, C. Yang, K. Han, S. Shaik, *J. Phys. Chem. B* **2007**, *111*, 7700–7710.
[19] J. N. Harvey, M. Aschi, *Faraday Discuss.* **2003**, *124*, 129–143.
[20] S. G. Ard, J. J. Melko, V. G. Ushakov, R. Johnson, J. A. Fournier, N. S. Shuman, H. Guo, J. Troe, A. A. Viggiano, *J. Phys. Chem. A* **2014**, *118*, 2029–2039.
[21] a) F. L. Hirshfeld, *Theor. Chem. Acc.* **1977**, *44*, 129–138; b) J. P. Ritchie, S. M. Bachrach, *J. Comput. Chem.* **1987**, *8*, 499–509.
[22] A. V. Marenich, S. V. Jerome, C. J. Cramer, D. G. Truhlar, *J. Chem. Theory Comput.* **2012**, *8*, 527–541.
[23] Gaussian 09, Revision C.01, M. J. Frisch, G. W. Trucks, H. B. Schlegel, G. E. Scuseria, M. A. Robb, J. R. Cheeseman, G. Scalmani, V. Barone, B. Mennucci, G. A. Petersson, H. Nakatsuji, M. Caricato, X. Li, H. P. Hratchian, A. F. Izmaylov, J. Bloino, G. Zheng, J. L. Sonnenberg, M. Hada, M. Ehara, K. Toyota, R. Fukuda, J. Hasegawa, M. Ishida, T. Nakajima, Y. Honda, O. Kitao, H. Nakai, T. Vreven, J. A. Montgomery, J. E. Peralta, F. Ogliaro, M. Bearpark, J. J. Heyd, E. Brothers, K. N. Kudin, V. N. Staroverov, R. Kobayashi, J. Normand, K. Raghavachari, A. Rendell, J. C. Burant, S. S. Iyengar, J. Tomasi, M. Cossi, N. Rega, J. M. Millam, M. Klene, J. E. Knox, J. B. Cross, V. Bakken, C. Adamo, J. Jaramillo, R. Gomperts, R. E. Stratmann,

O. Yazyev, A. J. Austin, R. Cammi, C. Pomelli, J. W. Ochterski, R. L. Martin, K. Morokuma, V. G. Zakrzewski, G. A. Voth, P. Salvador, J. J. Dannenberg, S. Dapprich, A. D. Daniels, Ö. Farkas, J. B. Foresman, J. V. Ortiz, J. Cioslowski, D. J. Fox, Gaussian, Inc., Wallingford, CT, **2009**.

[24] a) F. Weigend, R. Ahlrichs, *Phys. Chem. Chem. Phys.* **2005**, *7*, 3297 – 3305; b) F. Weigend, *Phys. Chem. Chem. Phys.* **2006**, *8*, 1057 – 1065.

[25] M. W. Schmidt, K. K. Baldridge, J. A. Boatz, S. T. Elbert, M. S. Gordon, J. H. Jensen, S. Koseki, N. Matsunaga, K. A. Nguyen, S. Su, T. L. Windus, M. Dupuis, J. A. Montgomery, *J. Comput. Chem.* **1993**, *14*, 1347 – 1363.

[26] a) S. Koseki, M. W. Schmidt, M. S. Gordon, *J. Phys. Chem.* **1992**, *96*, 10768 – 10772; b) D. G. Fedorov, S. Koseki, M. W. Schmidt, M. S. Gordon, *Int. Rev. Phys. Chem.* **2003**, *22*, 551 – 592.

[27] Gaussrate 2009 A, J. Zheng, S. Zhang, J. C. Corchado, Y.-Y. Chuang, E. L. Coitiño, B. A. Ellingson, D. G. Truhlar, University of Minnesota, Minneapolis, MN, **2010**.

[28] Polyrate 2010 A, J. Zheng, S. Zhang, B. J. Lynch, J. C. Corchado, Y.-Y. Chuang, P. L. Fast, W.-P. Hu, Y.-P. Liu, G. C. Lynch, K. A. Nguyen, C. F. Jackels, A. F. Ramos, B. A. Ellingson, V. S. Melissas, J. Villà, I. Rossi, E. L. Coitiño, J. Pu, T. V. Albu, R. Steckler, B. C. Garrett, A. D. Isaacson, D. G. Truhlar, University of Minnesota, Minneapolis, MN, **2010**.

[29] B. C. Garrett, T. Joseph, T. N. Truong, D. G. Truhlar, *Chem. Phys.* **1989**, *136*, 271 – 293.

[30] Y. P. Liu, G. C. Lynch, T. N. Truong, D. H. Lu, D. G. Truhlar, B. C. Garrett, *J. Am. Chem. Soc.* **1993**, *115*, 2408 – 2415.

[31] a) A. Fernandez-Ramos, B. A. Ellingson, B. C. Garrett, D. G. Truhlar in *Reviews in Computational Chemistry*, *Vol. 23* (Eds.: K. B. Lipkowitz, T. R. Cundari), Wiley-VCH, Hoboken, NJ, **2007**, pp. 125 – 232; b) D. G. Truhlar, A. D. Isaacson, B. C. Garrett in *Theory of Chemical Reaction Dynamics*, *Vol. 4* (Ed.: M. Baer), CRC, Boca Raton, FL, **1985**, pp. 65 – 137; c) B. C. Garrett, D. G. Truhlar, in *Theory and Applications of Computational Chemistry: The First Forty Years* (Eds.: C. E. Dykstra, G. Frenking, K. S. Kim, G. E. Scuseria), Elsevier, Amsterdam, **2005**, pp. 67 – 87.

Received: November 21, 2014
Revised: January 8, 2015
Published online: February 4, 2015

